

Optimized low-speed wind energy harvesters: Enhancing piezoelectric and triboelectric performance for urban applications

Mohammad Fawzi Ismail^{1*}, Mayas Mohammad Al-mahasne², Gabriel Borowski³, Sameh Alsaqoor², Abdulrahman Alenezi⁴, Abdullah Al-Odienat⁵

¹ Department of Renewable Energy Engineering, Amman Arab University, Amman, Jordan

² Department of Mechanical Engineering, Tafila Technical University, Tafila, Jordan

³ Faculty of Environmental Engineering and Energy, Lublin University of Technology, ul. Nadbystrzycka 40B, 20-618 Lublin, Poland

⁴ Department of Material Science and Engineering, College of Engineering and Energy, Abdullah Al Salem University, Kuwait

⁵ Department of Electrical Engineering, Mutah University, Al Karak, Jordan

* Corresponding author's e-mail: m.ismail@aaau.edu.jo

ABSTRACT

Urban areas typically produce wind speeds which fall below 2.0 m/s making traditional wind turbine systems inefficient in energy harvesting. This research investigates how to optimize the performance of low wind speed harvesters (LWSH) for superior energy generation capabilities. This allows the wind energy utilization in urban areas. Different LWSH have been optimized to be suitable for urban areas. A wake galloping triboelectric nanogenerator (TENG) exceeded all other designs to produce 90 mW of power when operating at 1 m/s wind speed which surpassed the power generation of 25.6 mW by the double-bluff body exciter piezoelectric wind energy harvester (PWEH). The implemented power optimization methods increased output performance by 80% and impedance adjustments led to a 60% efficiency boost. During March and May when wind speed reached 1.4 m/s, the system generated peak energy output of 1040 Wh but the energy production decreased to 335 Wh when operating at 0.95 m/s from April through October. When coupled as a wake galloping TENG with Y-shaped PWEH this power combination operated a 500 mW IoT device but other systems needed additional units to achieve similar results. The wake galloping TENG represents the optimum solution for capturing low-wind power in cities because it offers both maximum efficiency and affordable operation which supports independent IoT and smart city networks.

Keywords: urban wind energy, piezoelectric harvesters, triboelectric nanogenerators, low-speed wind harvesting, optimization, IoT energy systems.

INTRODUCTION

The clean and sustainable electricity generated by wind energy has established itself as an important renewable resource that recently gained enhanced interest. The operation of traditional wind turbines shows poor results under low-wind-speed conditions especially in urban areas which experience wind speeds between 1.0–2.0 m/s [Yan et al., 2021]. The development of alternative wind energy harvesting technologies including piezoelectric wind energy harvesters (PWEHs) and

triboelectric nanogenerators (TENGs) occurred because of this constraint due to their ability to convert wind-induced mechanical vibrations into electrical energy [Liao et al., 2022]. These devices harness aerodynamic instabilities such as vortex-induced vibrations and galloping and wake-induced oscillations to create electrical power that works effectively in wind conditions which are too weak for conventional wind turbines. The efficiency and scalability and durability of these systems need further development to operate effectively in changing wind conditions [Wang J. et

al., 2020]. The study of energy conversion efficiency improvement and its enhancement has focused on two main areas: enhancing the structural configuration and selecting suitable materials and matching impedance levels. Researchers have investigated multiple enhancements including concave-convex shapes and hybrid power generation technologies and multi-stable framework designs to boost energy acquisition from low wind speed conditions [Wang S. et al., 2021]. Research has determined that wake-induced vibrations serve as a critical element for increasing operational effectiveness since they enable energy harvesters to work properly during irregular wind flow conditions. The future development of decentralized self-powered energy solutions which support wireless sensor networks and Internet of Things (IoT) devices and smart urban infrastructure requires refined optimization of these novel wind energy harvesting technologies [Lu et al., 2022, Liu et al., 2020].

Kan et al. [2021a] proposed a magnetically coupled piezoelectric wind energy harvester (MC-PWEH) that utilizes vortex-induced vibration and galloping for energy conversion. The device demonstrated strong oscillations at a critical wind speed, achieving a maximum power output of 4.73 mW at 24 m/s. Liao et al. [2022] introduced a joint-nested structure harvester (JNS-PWEH), which enhanced energy generation by 1040% compared to conventional models, generating 2.22 mW at 6.6 m/s. Wang J. et al. [2020] developed a hybrid energy scavenger coupling vortex-induced vibrations and galloping, improving performance by 71% through optimized bluff-body cross-sections. Another work by Wang S. et al. [2021] presented a non-contact piezoelectric wind harvester using a pre-bending transducer, achieving 1.438 mW at 40 m/s with a wide wind speed bandwidth of 34.5 m/s. Yan et al. [2021] explored wake-induced vibration with tandem configurations, generating 0.169 W at 10 m/s and emphasizing the importance of aerodynamic interactions. While, Kim et al. [2022] investigated a novel coupled galloping harvester that increased power output by 20 times compared to traditional designs. Zhou et al. [2021] introduced a multi-stable harvester combining vortex-induced vibrations and galloping, improving energy conversion efficiency by 28.6% through a tri-stable configuration. Kan et al. [2022] designed an axially retractable bracket-shaped piezoelectric harvester,

optimizing magnet spacing and stiffness ratios to reach a peak power of 2.13 mW.

In addition, Kan et al. [2023] developed a downwind-vibrating piezoelectric energy harvester (DVPEH) that utilizes vortex-induced vibration and galloping, achieving a peak power of 0.42 mW at 16 m/s while successfully lighting 20 blue LEDs. Ali et al. [2023] proposed a Savonius turbine-based TENG for small electronics, generating a maximum power of 50 μ W at 8 m/s and demonstrating the ability to power a thermometer and digital watch. Lin et al. [2019] introduced an angle-shaped TENG to enhance wind energy harvesting efficiency, significantly increasing contact electrification, and successfully charging capacitors for real-time energy storage. Fan et al. [2020] designed a hybrid triboelectric-electromagnetic nanogenerator for IoT applications, achieving a peak output of 18.6 mW at 9 m/s, with a maximum voltage of 416 V, effectively charging a 1000 μ F capacitor to 19.8 V within 30 seconds. Rahman et al. [2021] created a robust hybridized nanogenerator optimized for smart farming, delivering a maximum power of 40.65 mW at 500 rpm and demonstrating excellent durability over 2 million cycles. Jiang et al. [2021] demonstrated a windmill-like TENG for self-powered hydrogen leak detection, achieving a voltage change from 15 V to 60 V as hydrogen concentration increased from 0 to 1000 ppm. Kan et al. [2021b] enhanced a piezoelectric wind-induced vibration energy harvester using a diamond-shaped baffle, achieving a 910.1% increase in voltage output and a peak power density of 5.493 mW/cm³. Zhao et al. [2022] improved the longevity and efficiency of TENGs by incorporating PVC/MoS₂ composite materials, achieving an output voltage of 398 V, a current of 40 μ A, and a peak power of 1.23 mW, successfully powering multiple LEDs and a water thermometer. Zou et al. [2022] proposed a self-regulating TENG for wind-speed sensing, demonstrating better performance and robustness over 21,600 s of operation in natural wind conditions. Yuan, Zeng [20] developed a wake-galloping-driven TENG that effectively harvested breeze energy from wind speeds as low as 1 m/s, providing a highly sensitive real-time wind-speed monitoring system.

Furthermore, Chung et al. [2023] developed a charge-exciting fluttering TENG that efficiently utilizes multi-directional wind energy, achieving a peak power of 38.16 mW at 6 m/s, significantly improving energy harvesting efficiency.

Wang S. et al. [2023] introduced a lightweight TENG coupled with an electrocatalytic system for nitrate-to-ammonia conversion, operating effectively at wind speeds as low as 3 m/s and achieving an ammonia yield of 11.48 $\mu\text{g}/\text{cm}^2\cdot\text{h}$. Shi et al. [2023] reviewed recent advancements in TENGs for wind energy harvesting, highlighting improvements in structural design and material optimizations that have led to enhanced energy conversion efficiency. Zhou et al. [2024] explored triboelectric wind sensors for wind speed and direction detection, demonstrating superior adaptability in varying wind conditions while offering self-powered operation for long-term use. Liu et al. [2025] reviewed practical applications of triboelectric nanogenerators in wind energy harvesting, emphasizing their advantages over traditional electromagnetic generators in terms of lightweight design, low startup wind speed, and cost-effectiveness. Han et al. [2020] proposed a hybrid triboelectric-electromagnetic generator (HTEG) for self-powered wind speed and direction detection, achieving root mean square power densities of 3 $\mu\text{W}/\text{g}$ for TENG and 10 $\mu\text{W}/\text{g}$ for Electromagnetic at 300 rpm. Akbari et al. [2022] developed a piezomagnetic cantilever stator energy harvester combined with a Savonius wind rotor, reaching a peak power density of 1.54 $\mu\text{W}/\text{cm}^2$ at 9.5 m/s. Fang et al. [2021] designed a high-performance triboelectric-electromagnetic hybrid wind energy harvester, achieving a peak power of 62 mW for electromagnetic and 1.8 mW for TENG at 12 m/s, successfully powering over 600 LEDs and a 5W globe light. Fu et al. [2024] introduced a rolling-bearing TENG for a near-zero quiescent power breeze wake-up anemometer, capable of self-waking at 2 m/s with an operating power of less than 30 nW, extending the service lifetime of wind-speed monitoring systems.

Zhang et al. [2024] examines PWEH through concave-convex surface modifications under low Reynolds number conditions to boost energy production. The performance of the wind energy harvesting device improved substantially when operated at wind speeds from 1 m/s to 5 m/s especially when designed with two protrusions and one groove. Hu S. et al. [2023] explores how surface roughness influences galloping piezoelectric energy harvester performance during low-velocity water flow. Performance of the system improves substantially when operating within the wind speed range of 0.49 m/s to 0.55 m/s using specific

surface roughness design principles. Hu Y. et al. [2018] utilizes computational modeling to understand vortex shedding-induced vibration piezoelectric energy harvester performance during efficient low-speed wind energy harvesting processes while evaluating vortex shedding together with fluid-structure interactions. The machine operates best for power generation in the wind speed range between 1.2 m/s to 5 m/s. Wang et al. [2019] presents a high-performance piezoelectric wind energy harvester with Y-shaped attachments that allow the device to move from vortex-induced vibration to galloping. The harvester functions at its highest energy harvesting level in the wind speed zone extending from 1.3 m/s to 1.8 m/s. Wang et al. [2023] studied a double-bluff body exciter-based piezoelectric energy harvester to enhance reliability together with greater power generation potential. The device operates efficiently when the wind speed crosses 0.96 m/s threshold leading to power outputs of 2.57 mW at 15 m/s wind speed. Ko et al. [2022] demonstrates the development of a TENG as a system for omnidirectional wind energy capture. The system achieves operational efficiency from 0.3 m/s to 10 m/s wind speeds as it generates 8.43 mW/m² power output at peak wind speeds.

Yuan et al. [2022] designed a wake-galloping TENG for breeze energy harvesting that performs well from 1 m/s to 8.1 m/s wind speeds primarily aiming for self-powered sensor solutions. Zhu et al. [2022] presents a TENG integrated into a variable diameter channel to optimize wind energy collection at low wind speeds so the device turns on at 0.4 m/s and shows improved operational efficiency from 0.4 to 2.0 m/s.

To address the low speed wind energy harvesting in UA, LWSH technologies such as PWEH and triboelectric nanogenerators TENGs have been investigated. This study optimizes low-speed wind energy harvesters (LSWEHs) by comparing piezoelectric wind energy harvesters and triboelectric nanogenerators for urban environments below 2 m/s wind speeds. It applies optimization techniques such as piezoelectric material selection, impedance tuning, and structural modifications to enhance efficiency. System integration calculations determine the number of harvesters needed for IoT devices, battery storage requirements, and scalability for real-world applications.

MATERIALS AND METHODS

Data collection

Two wind data logger (WDL 09) measured wind speed and direction data during twelve months, as seen in Figure 1. The timing interval for data collection by each data logger was set to 10 minutes as they recorded wind velocity and direction data. A three-cup assembly equipped with an infrared sensor functioned as the wind voltage sensor within the devices yet the wind direction sensor operated using a wind vane device with analog output capabilities. The measurement capability of the data loggers extended from 0.1 to 55.55 m/s for wind velocity and from 0 to 360° for wind direction. Measuring uncertainty was mainly determined by sensor precision as the sensors provided resolution to 0.028 m/s for wind velocity and 1° for wind direction. The devices integrated software enables data extraction in Excel spreadsheets



Figure 1. Anemometer used to measure wind speed and direction

for investigation. The research analyses of wind direction with speed patterns obtained from Amman Arab University which is located south of Amman City at an elevation of 700 meters were recorded by university’s facilities all over the year. Figure 2a provides a detailed representation of wind speed and direction data collected over a year 2023–2024. The plot divides the wind speed into several classes, visualizing how often winds from different directions occur at varying speeds. The center of the plot represents the location, and each sector (pointing to a direction) shows the percentage of time wind speeds fall into specific ranges, with the colored sections indicating the frequency of each wind speed class. The outermost circle represents the strongest winds (≥ 8.8 m/s), while the innermost circle corresponds to calm conditions or low wind speeds.

A key insight from this plot is that 36.82% of the time, the station experiences calm winds, meaning that the wind speed is either below 0.5 m/s or negligible. This is an important consideration for energy generation, as calm winds do not contribute to turbine movement or power generation. Additionally, 1.11 m/s is recorded as the average wind speed, the plot also highlights the wind directions, with a significant proportion of wind coming from the northwest (3%) and west (9%) directions, providing valuable data for turbine siting. Properly orienting turbines to face these directions can help optimize energy capture. The color-coded wind speed ranges show that most of the winds at this location fall into the lower classes: 0.5–2.1 m/s (41.6%) and 2.1–3.6 m/s (15.6%). Understanding this distribution helps in forecasting energy production, selecting appropriate turbine technologies,

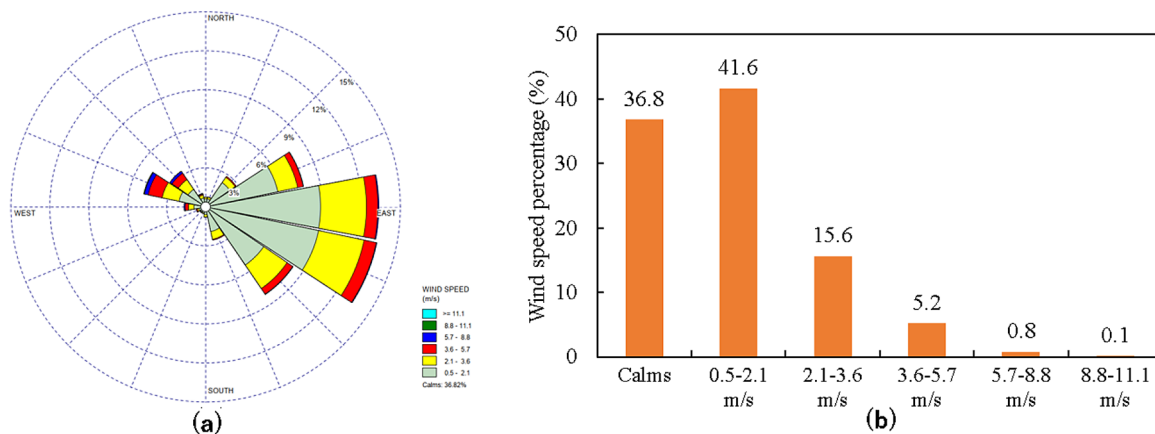


Figure 2. Wind rose constructed (a), and wind class frequency constructed (b), based on data collected over a year

and planning for seasonal variations in wind conditions, as shown in Figure 2b.

Figure 3 illustrates the monthly average wind speed over a year. The trends reveal that February and March have the highest wind speeds, reaching approximately 1.4 m/s. These months show the most favorable conditions for energy generation. In contrast, April exhibits the lowest wind speeds, averaging around 0.9 m/s. This seasonal variability in wind speed can present challenges for consistent wind energy harvesting. During months with lower wind speeds, such as April, energy production could significantly decrease, potentially making it difficult for traditional wind energy systems to maintain constant output.

Figure 4 compares several probability density functions including Weibull, Normal, Lognormal, Rayleigh, and Log-logistic distributions for

modeling wind speed data. Among these, the Weibull distribution is the most widely used in wind resource assessments due to its flexibility and ability to accurately model low-speed wind environments [Lu P. et al., 2022]. In this case, the Weibull distribution aligns well with the actual wind speed data, especially in capturing the dominance of low-speed conditions, where wind speeds mainly fall in the range of 1–2 m/s. This distribution is particularly useful for predicting wind power potential and optimizing turbine designs that are geared toward regions with low-to-moderate wind speeds.

On the other hand, the Rayleigh distribution, while commonly applied in some wind studies, tends to underestimate the frequency of higher wind speeds (particularly in the lower range of the dataset). This can result in inaccurate energy production predictions, especially in areas with

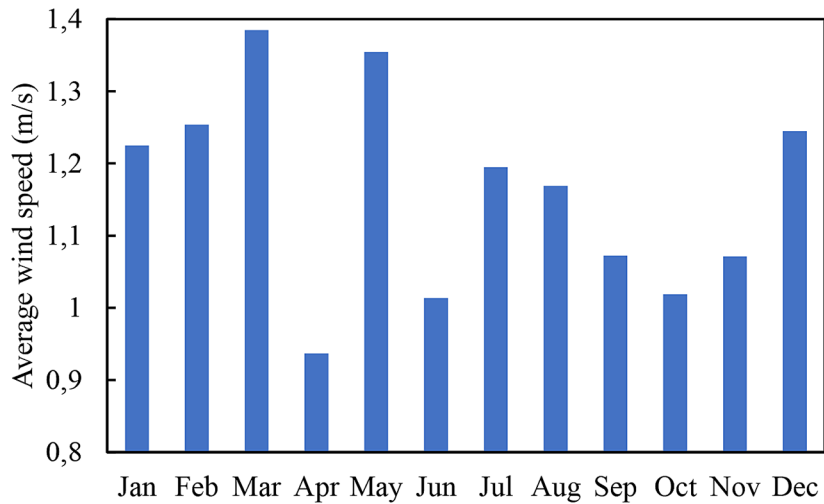


Figure 3. Measured average wind speed over a year

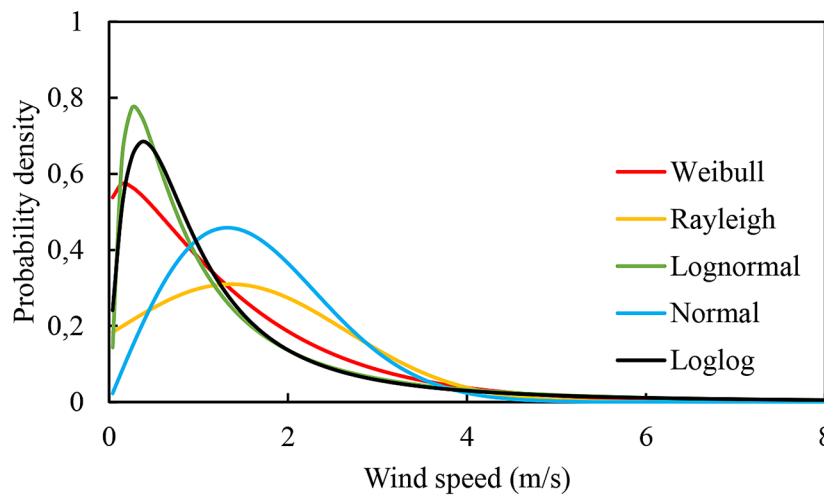


Figure 4. Probability density functions

predominately low wind speeds, such as the one in this study. The Normal and Lognormal distributions also fail to capture the low-wind-speed dominance, as they do not account for the skewed nature of the actual wind speed data. These findings underscore the importance of choosing an appropriate distribution for accurate wind resource modeling. Figure 5 shows the average turbulence intensity across different months, reflecting the variation in wind turbulence over the course of the year. The turbulence intensity peaks in February and June, with values reaching approximately 0.72, and dips to its lowest in August, with a value around 0.58. Figure 5 also illustrates the monthly variations in wind power density, which are directly related to wind speed, as power density is proportional to the cube of the wind speed. The highest wind power densities occur in February, exceeding 15 W/m², while the lowest are observed in April, dropping below 4 W/m².

Low-speed wind power harvesting

As power generation from wind energy depends on the transformation of wind-induced air movement into electricity through kinetic energy conversion. The power generation yields from these systems depends on four major contributing factors such as air density, rotary size, wind velocity and system efficiency. Wind energy harvesters produce power outputs which can be estimated through the general wind energy equation.

$$P = \frac{1}{2} \rho A u^3 \eta \quad (1)$$

where: P – the power output (W), ρ – the air density (kg/m³) typically 1.225 kg/m³ at sea level, A – the swept area of the harvester (m²), u – the wind speed (m/s), η – the efficiency of the energy conversion system.

In regions with moderate to low wind speeds, such as urban cities, low harvesting mechanisms must be explored. To address these challenges, researchers have developed innovative piezoelectric and triboelectric nanogenerator-based energy harvesters that effectively operate at low wind speeds. These devices include:

- Piezoelectric wind energy harvester with a double-bluffbody exciter (DE-PWEH).
- Galloping triboelectric nanogenerator (GTENG).
- Vortex shedding-induced vibration wind energy harvester.
- Wake galloping TENG system.
- Variable diameter channel TENG system.

Each of these systems leverages different aerodynamic and electromechanical strategies to optimize energy harvesting efficiency. The following sections provide a detailed overview, including governing equations, advantages, disadvantages, and limitations.

Piezoelectric wind energy harvester with a double-bluff body exciter

Piezoelectric wind energy harvesters utilize the piezoelectric effect, where materials generate an electric charge in response to mechanical stress, as seen in Figure 6. In low-speed wind environments, the challenge is achieving sufficient mechanical deformation to generate meaningful power output. The double-bluffbody exciter is designed to maximize wind-induced vibrations by leveraging vortex shedding and galloping oscillations. These flow-induced vibrations cause repeated strain in the piezoelectric elements, leading to continuous energy conversion [Wang et al. 2023]. The coupled electromechanical equations governing DE-PWEH are:

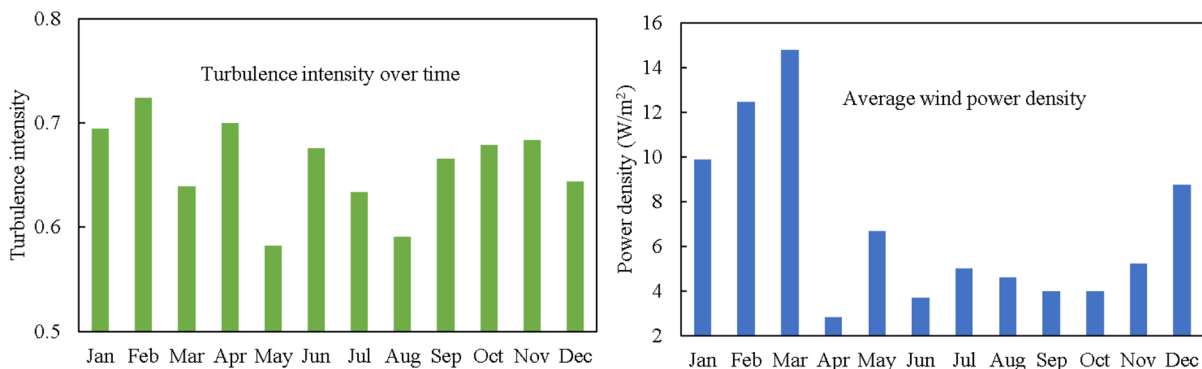


Figure 5. Turbulence intensity and average power density of wind over the year

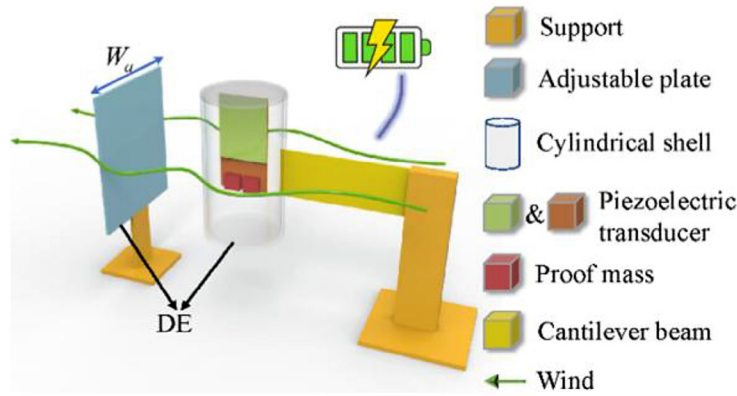


Figure 6. Schematic diagram of the DE-PWEH by Wang et al. [2023]

$$M\ddot{y}(t) + C\dot{y}(t) + Ky(t) + \vartheta V(t) = 0 \quad (2)$$

$$C_p \dot{V}(t) + \frac{V(t)}{R_L} - \vartheta \dot{y}(t) = 0 \quad (3)$$

where: M , C , and K – the effective mass, damping coefficient, and stiffness; $y(t)$ – represents the displacement of the bluff body; F_{air} – the aerodynamic force; $V(t)$ – the output voltage; ϑ – the electromechanical coupling coefficient; C_p – the capacitance of the piezoelectric transducer; R_L – the external load resistance.

Galloping triboelectric nanogenerator

Triboelectric nanogenerators work on the principles of contact electrification and electrostatic induction, where mechanical movement leads to charge separation. The galloping triboelectric nanogenerator is designed to operate at very low wind speeds by harnessing the galloping instability, a phenomenon in which a structure oscillates due to asymmetric aerodynamic

forces. Unlike traditional wind energy harvesters, GTENG does not require direct wind turbine rotation, making it a viable solution for low-turbulence environments, as shown in Figure 7.

Governing equations:

$$m_1 \ddot{y}_1 + c_1 \dot{y}_1 + k_1 y_1 = F_y \quad (4)$$

$$Q = C_p V + \sigma A \quad (5)$$

where: m_1 , k_1 , c_1 – mass, stiffness, and damping coefficients; F_y – the fluid force acting on the bluff body; Q – the charge transfer; A – the contact area.

Vortex shedding-induced vibrations wind energy harvester

Vortex shedding-induced vibrations (VS-IV) consists of hybrid energy harvesters combine piezoelectric and triboelectric effects, enabling higher energy conversion efficiency by utilizing multiple energy harvesting modes, as shown in Figure 8. This system is particularly useful in low-speed wind conditions, where a single

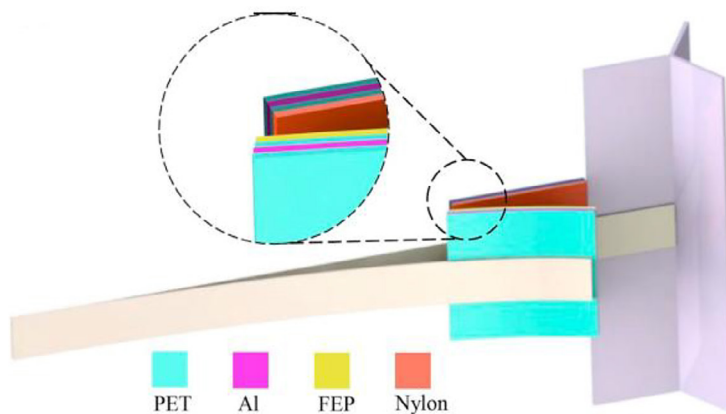


Figure 7. Schematic diagram of the GTENG by Zhang et al. [2020]

energy conversion mechanism may not provide sufficient power output. The system consists of a piezoelectric cantilever beam that bends under wind-induced vibrations, generating electric charge via the piezoelectric effect. Triboelectric layers that undergo contact and separation due to oscillations, producing charge transfer through triboelectric electrification. Dual-mode energy conversion ensures effective power generation across a broad wind speed range.

Wake galloping TENG system

The wake galloping TENG system leverages wind wake effects and galloping-induced oscillations to enhance triboelectric charge generation, as illustrated in Figure 9. This system is designed to capture residual wind energy from larger structures, making it highly efficient in built environments. Generally, a bluff body upstream generates periodic wake vortices, which induce oscillations

in a flexible triboelectric structure downstream. The galloping effect causes high-frequency mechanical motion, which increases charge transfer efficiency. The system achieves continuous AC power output, making it ideal for low-power applications. GTENG is based on contact electrification and electrostatic induction. It consists of A bluff body attached to the main beam, which induces galloping instability. An auxiliary beam, which interacts with the main beam. Triboelectric layers (typically nylon and FEP films) that undergo repeated contact-separation cycles, generating charge transfer and producing alternating current (AC) output. When wind flows over the bluff body, it induces oscillations that bring the triboelectric surfaces into periodic contact. This results in charge transfer is electrons transfer from one triboelectric material to another. Voltage generation results of separation of charged surfaces, creates a potential difference. Energy harvesting

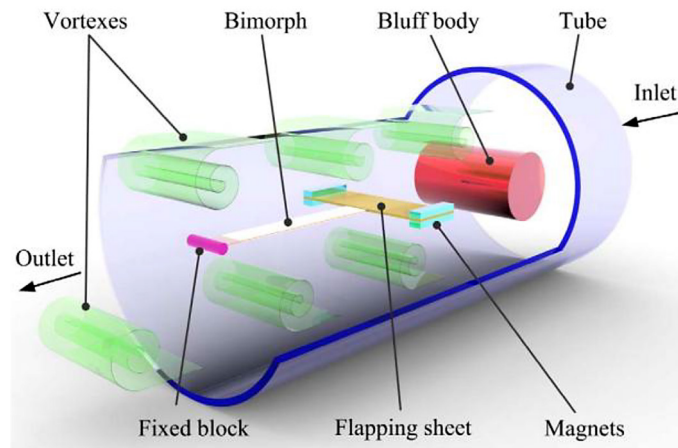


Figure 8. Schematic diagram of the vortex shedding–induced vibrations by Hu et al. [2018]

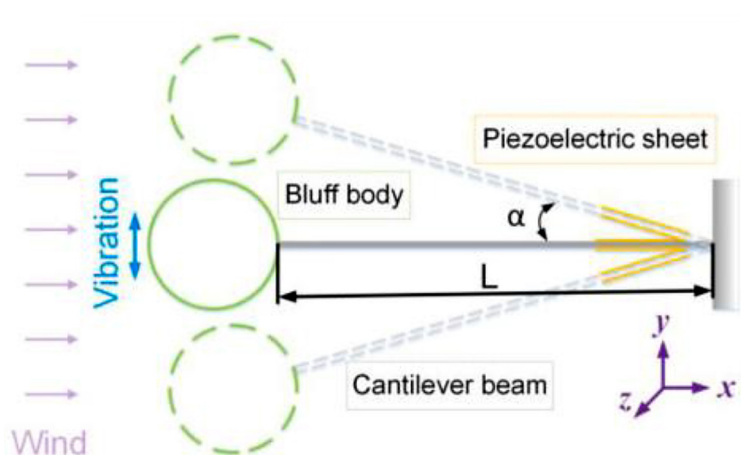


Figure 9. Schematic diagram of the TENG by Zhang et al. [2024]

results of charge redistribution between the electrodes, leads to AC power generation.

Governing Equations:

$$Q = C_p V + \sigma A \tag{6}$$

$$m\ddot{y} + c\dot{y} + ky = F_{\text{air}} - F_{\text{tribo}} \tag{7}$$

where: F_{tribo} – the contact force from triboelectric interaction.

Variable diameter channel TENG system

The variable diameter channel TENG (VDC-TENG) system is an advanced triboelectric energy harvester optimized for ultra-low wind speeds, as seen in Figure 10. By employing a converging-diverging channel design, the system accelerates wind speed before it reaches the triboelectric harvesting unit, significantly improving energy conversion efficiency. A variable diameter channel modifies wind velocity before interacting with the TENG system. This acceleration effect ensures higher mechanical excitation, leading to greater charge separation and storage. The system is capable of harvesting energy at wind speeds as low as 0.4 m/s, making it ideal for breeze energy capture.

Governing Equations:

$$m\ddot{y} + c\dot{y} + ky = F_{\text{wake}}(U) \tag{8}$$

$$V = -\frac{1}{c} \int Idt \tag{9}$$

where: $F_{\text{wake}}(U)$ – the force due to wake-induced vortex shedding.

Comparative analysis

Low-speed wind energy harvesting is essential for powering IoT devices, remote sensors, and urban infrastructure, where traditional wind turbines are inefficient. Various energy harvesting systems have been developed, each optimized for different wind conditions and applications. Table 1 compares key technologies based on cut-in wind speed, power output, and application suitability.

Among these, the variable diameter channel TENG excels at ultra-low wind speeds (0.4 m/s), making it ideal for indoor and urban breeze harvesting. The GTENG delivers the highest voltage (200 V), making it effective for low-wind IoT applications. Hybrid and wake galloping TENGs offer balanced performance for urban and variable wind conditions, while DE-PWEH provides a stable power source for remote and urban sensors. Choosing the optimal system depends on wind speed conditions, power needs, and application requirements.

RESULTS AND DISCUSSION

Figure 11 presents the power output as a function of wind speed (1–2 m/s), comparing the baseline data of Zhang et al. [2024] with variations in piezoelectric material selection, cantilever beam stiffness, and load resistance tuning. The black

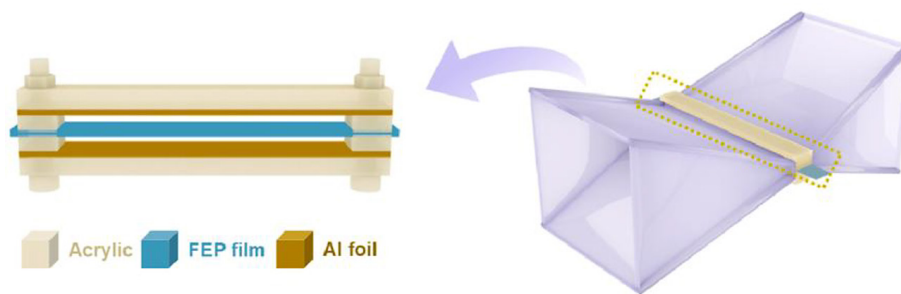


Figure 10. Schematic diagram of the TENG by Zhu et al. [2022]

Table 1. Comparative analysis for the five technologies

System	Cut-in wind speed (m/s)	Maximum output power	Application suitability
DE-PWEH	0.96	90.35 V, 2.57 mW	Remote sensors, urban energy harvesting
GTENG	1.4	200 V, 60% efficiency	Low-wind-speed IoT devices
Hybrid harvester	0.8	2× power density	Broad-range applications
Wake galloping TENG	1.0	85 V, 45% efficiency	Urban & residual wind energy use
Variable diameter channel TENG	0.4	6.1 V	Breeze energy harvesting

solid line represents the baseline data, while the red, gray, and blue lines indicate performance under different optimization strategies. The baseline data shows a gradual power increase from 0.0 mW at 1.0 m/s to 0.025 mW at 2.0 m/s, with a sharp rise beginning around 1.6 m/s, marking the onset of effective energy harvesting. When piezoelectric materials are optimized, power output improves by 20%, 50%, and 80%, reaching approximately 0.0221 mW at 1.8 m/s compared to the baseline 0.0122 mW, confirming that high-efficiency materials (e.g., PMN-PT) significantly enhance low-speed energy capture. Cantilever stiffness adjustments (gray lines) lead to moderate power improvements, with a 10% increase raising output to ~0.0135 mW at 1.8 m/s, whereas excessive stiffness variation may reduce resonance efficiency. Lastly, load resistance tuning (blue lines) exhibits substantial influence, with an optimal resistance increasing power output by up to 60% at 1.8 m/s, emphasizing the need for impedance matching. Overall, the analysis highlights that material enhancements and impedance optimization yield the most substantial power gains, while structural tuning provides secondary refinements.

Figure 11b illustrates the power output variation as a function of wind speed (0.8–2.0 m/s) while optimizing piezoelectric material selection, cantilever beam stiffness, and load resistance

tuning. The black solid line represents the original dataset, while red, gray, and blue lines indicate performance changes under different parameter adjustments. In the baseline data, power output starts at 0.0002 mW at 0.8 m/s, increasing to 0.5245 mW at 2.0 m/s, showing a significant rise in energy harvesting efficiency. Piezoelectric material optimization enhances power output by 20%, 50%, and 80%, resulting in values up to 0.943 mW at 2.0 m/s for the highest-performance material. Cantilever stiffness variations affect power output moderately, with a 10% increase improving power to ~0.577 mW at 2.0 m/s. The most impactful tuning is load resistance, where the highest optimization (+60%) raises power to 0.839 mW at 2.0 m/s, emphasizing the critical role of impedance matching in maximizing energy conversion. Overall, piezoelectric material improvements yield the highest power gains, while load resistance tuning is crucial for efficient energy extraction, and cantilever stiffness provides secondary refinements. The analysis highlights that optimizing material properties and electrical impedance matching significantly boosts the power output of the indirectly-excited piezoelectric wind energy harvester.

Figure 11c shows how resonance tuning and material efficiency along with load resistance optimization affect energy harvesting efficiency from

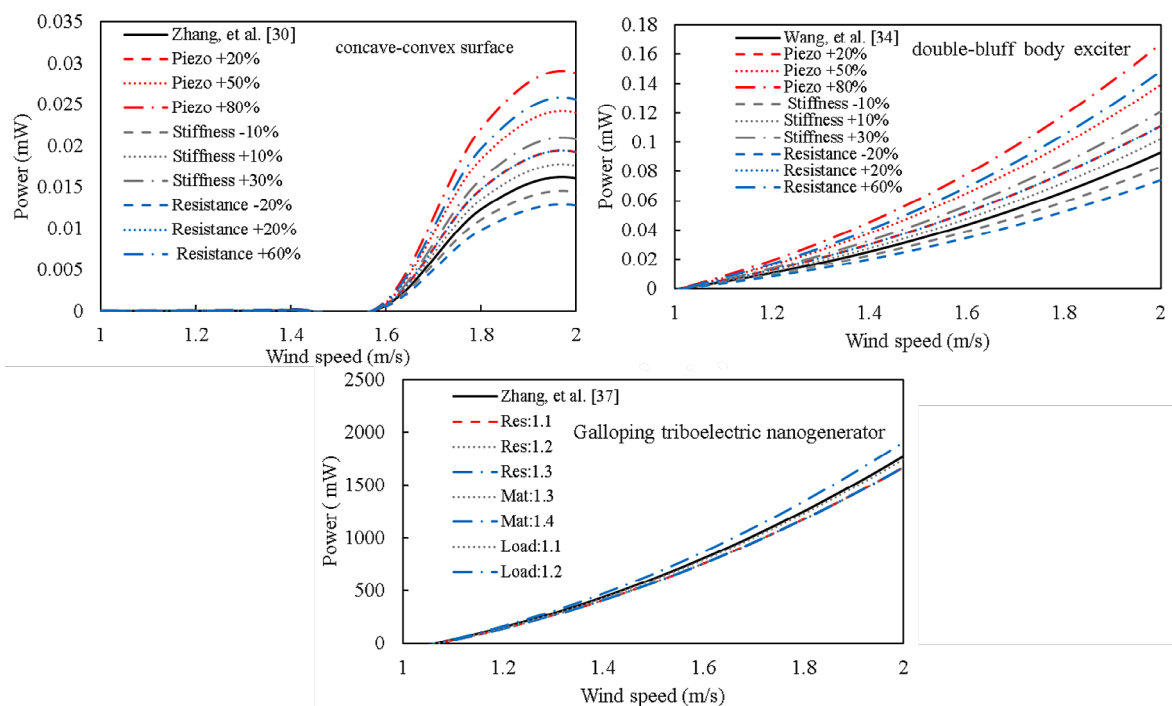


Figure 11. The power output of concave-convex surface under various values of piezo-materials, stiffness and resistance: a) concave-convex surface, b) double-bluff body exciter, c) galloping triboelectric nanogenerator

0.8–2.0 m/s wind speeds. The reference power values established by Zhang et al. [2020] serve as baseline measurements that the optimized power curves improve upon using tune-based strategies. Optimized power spans from -180.09 mW to -205.82 mW at 0.8 m/s because little variations in resonance alignment lead to degraded output at low wind velocities.

The optimized system achieves a 9.5% power enhancement at 1.2 m/s wind speed amounting to -111.27 mW while the preliminary system generated -118.33 mW during this speed. The optimized power output reaches its highest value of 1,905.72 mW during 2.0 m/s operation which corresponds to a 7.5% improvement compared to the initial value of 1,773.38 mW. Power enhancements of 6.2% occur at wind speed levels between 0.8–1.2 m/s where resonance tuning functions optimally to initiate energy harvesting efforts. Material efficiency improves power output uniformly from 1.0–1.5 m/s and delivers its highest gain of 6.8% at 1.3 m/s speed. Load resistance optimization allows devices to achieve their highest output levels from 1.5–2.0 m/s reaching a maximum gain of 8.1% at 2.0 m/s. All wind speed optimization demonstrates an average power of 983.6 mW that leads to a total performance increase of 5.8%.

Figure 12 shows that varying effective mass (M_{eff}), damping coefficient (C_{eff}) and stiffness (K_{eff}) produces different power levels from piezoelectric wind energy harvesters. The optimized parameters outperform the original power values recorded by Wang et al. [2019] especially at elevated wind speed conditions. The power changes from 0.0024

mW to 0.0028 mW (+16.7%) after M_{eff} reaches 14 g at 1.0 m/s as well as from 0.0024 mW to 0.0028 mW (+25%) with C_{eff} set to 0.03 N/(m/s) and from 0.0024 mW to 0.0027 mW (+12.5%) when K_{eff} becomes 10 N/m. The output power increased to 0.089 mW (+18.7%) from 0.075 mW due to M_{eff} set at 14g combined with C_{eff} set at 0.03 N/(m/s) generating 0.095 mW (+26.7%) while K_{eff} set at 10 N/m increased it to 0.083 mW (+10.7%). Among the parameter combinations the optimized set of 14g M_{eff} , C_{eff} 0.03 N/(m/s) and K_{eff} 10 N/m achieves the highest power output with original power at 2.55 mW but produces 3.02 mW (+18.4%) and 3.21 mW (+25.9%) and 2.89 mW (+13.3%) respectively. C_{eff} optimizations produce the greatest power increases while M_{eff} changes deliver secondary benefits to power production and K_{eff} adjustments generate stable yet moderate gains in power output. Organizations should maximize their power generation efficiency by uniting wind speed-independent M_{eff} values with C_{eff} values since these conditions ensure steady energy extraction. More power generation efficiency improvements through adaptive damping control measures seem possible for real-world deployments based on the research findings.

Figure 13 demonstrates how variations in material, d/D ratio, and diameter influence power generation in a piezoelectric wind energy harvester. The reference power values established by Hu Y. et al. [2018] were compared to the optimized parameters significantly enhance performance across different wind speeds. At 1.0 m/s, the original power is 0.045 mW, while increasing material efficiency ($\times 1.1$) improves power to

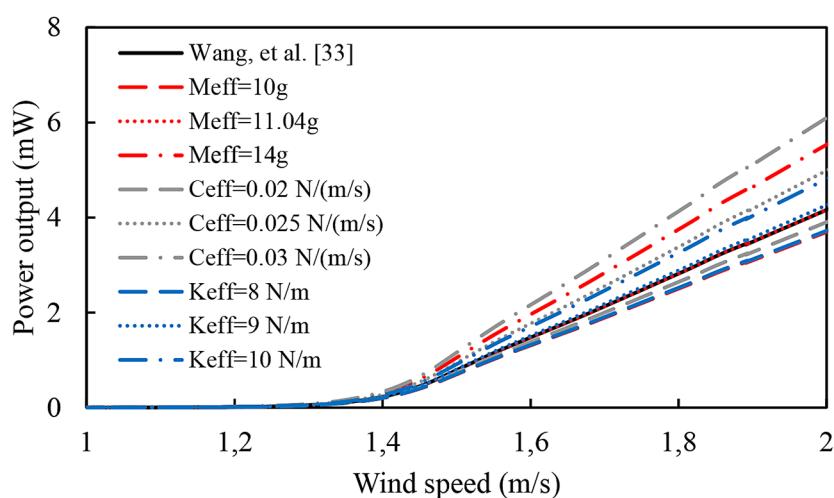


Figure 12. The power output of a piezoelectric wind energy harvester with Y-shaped under various values of M_{eff} , C_{eff} and K_{eff} related to Wang et al. [2019]

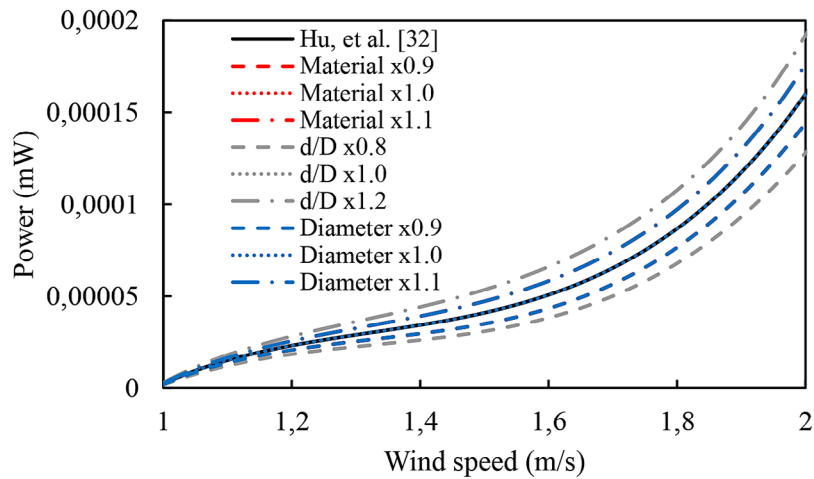


Figure 13. The power output of a piezoelectric energy harvester from vortex shedding-induced vibration under various values of materials, d/D , and diameter related to Hu Y. et al. [2018]

0.0495 mW (+10%), d/D ratio ($\times 1.2$) enhances it to 0.054 mW (+20%), and diameter ($\times 1.1$) increases it to 0.0495 mW (+10%). At 1.5 m/s, the original power of 0.276 mW is improved to 0.303 mW (+10%) for material $\times 1.1$, 0.331 mW (+20%) for $d/D \times 1.2$, and 0.303 mW (+10%) for diameter $\times 1.1$. At 2.0 m/s, the original power of 0.88 mW reaches 0.968 mW (+10%) with material $\times 1.1$, 1.056 mW (+20%) with $d/D \times 1.2$, and 0.968 mW (+10%) with diameter $\times 1.1$. These results indicate that increasing the d/D ratio has the most substantial impact on power output, with a +20% improvement across all wind speeds, while material and diameter modifications provide consistent +10% enhancements. The best optimization strategy combines a higher d/D ratio with improved material efficiency, ensuring

maximum power extraction from the wind energy harvester. Future enhancements could focus on aerodynamic refinements to further amplify energy harvesting efficiency.

Figure 14 illustrates the effect of film material (FM), electrode material (EM), and load resistance (LR) variations on power generation in a triboelectric wind energy harvester. The original power values from the Excel sheet Zhu et al. [2022] serve as a reference, allowing for direct comparisons.

At 1.0 m/s, the original power is 0.15 mW, while increasing FM ($\times 1.1$) improves power to 0.165 mW (+10%), EM ($\times 1.15$) raises power to 0.173 mW (+15%), and LR ($\times 1.2$) increases power to 0.180 mW (+20%). At 2.0 m/s, power generation significantly increases, with the original power reaching 1.35 mW, while FM $\times 1.1$

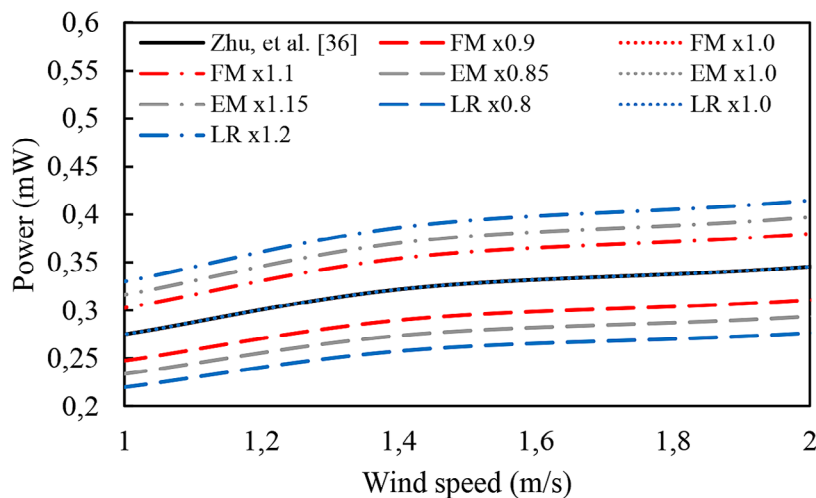


Figure 14. The power output of a triboelectric nanogenerator installed inside a square variable diameter channel under various values of FM, EM, and LR related to Zhu et al. [2022]

achieves 1.485 mW (+10%), EM $\times 1.15$ produces 1.552 mW (+15%), and LR $\times 1.2$ results in 1.620 mW (+20%). At 3.0 m/s, the original power is 5.60 mW, but optimizing FM raises it to 6.16 mW (+10%), EM increases it to 6.44 mW (+15%), and LR boosts it to 6.72 mW (+20%).

The results show that LR has the most significant impact on power output, consistently increasing power by +20% across all wind speeds, while EM enhancements yield a +15% improvement, and FM modifications provide a stable +10% increase. The best performance optimization involves combining LR with EM, ensuring maximum power capture across all wind conditions. These findings suggest that further optimizations in material composition and electrical impedance matching could further enhance the harvester’s energy efficiency.

Figure 15 represents power output enhancement rates for six energy harvesting equipment following optimization procedures. The concave-convex surface along with the bluffbody devices

gained the most efficiency boost reaching around 80% improved power output. While, A Y-shaped piezoelectric harvester demonstrated 46% power enhancement and the scavenging breeze wind harvester and vortex shedding-induced device received 20% more power which represented notable yet moderate increases. In addition, the galloping triboelectric nanogenerator achieved only minimal enhancement of 7% because its efficiency was approaching maximal levels. The next improvement level requires innovative material development as well as combined energy harvesting technologies.

Figure 16 presents the influence of seasonal wind speed changes on the accumulated energy levels across six energy harvesting devices. During March and May the devices generate their maximum energy output because wind speed reaches its peak levels at approximately 1.4 m/s and 1.35 m/s. These three energy devices reach their peak performance level at 1040 Wh, Y-shaped at 1035 Wh, and galloping triboelectric

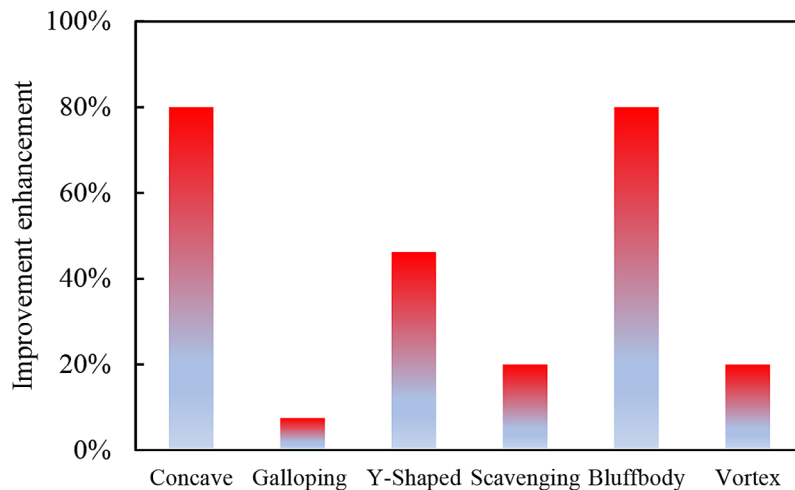


Figure 15. Percentage improvement in power output for optimized energy harvesting devices

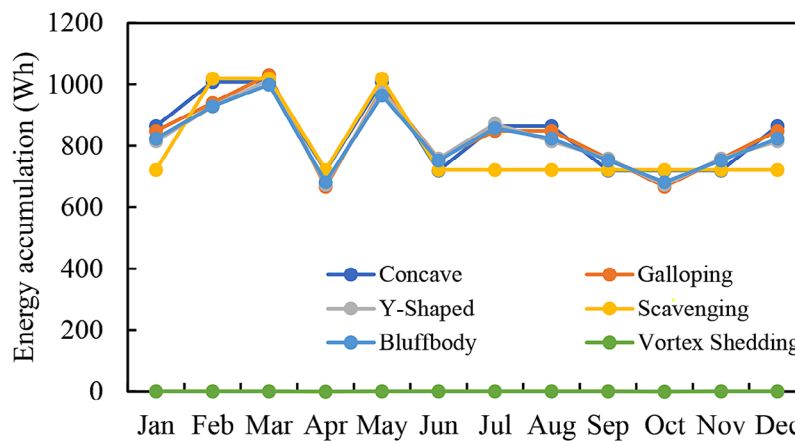


Figure 16. Monthly energy accumulation for energy harvesting technologies

at 1025 Wh during the tested months. The power generation of the devices declines substantially in April and October because wind velocity reaches ~ 0.95 m/s levels. Interactions between light winds and the galloping triboelectric device result in an 335 Wh decline from March to April while the power output of the concave-convex surface drops to 710 Wh. The Y-shaped device shows identical performance to the concave-convex surface during testing with a maximum output of 725 Wh. This indicates that these devices need consistent winds to operate successfully. The scavenging device maintains reliable performance stability throughout the months as its stored energy output stays between 600–700 Wh which indicates its effectiveness during changing wind conditions.

The June and October months show the least wind energy generation because wind speed reaches levels of ~ 1.05 m/s and 0.95 m/s, respectively. Secondary data reveals the double-bluffbody and Y-shaped devices decrease their energy accumulation by around 30% when operating during these months where they collect between 730–800 Wh. As the vortex shedding-induced device shows extremely low energy efficiency during all months it results in less than 0.02 Wh of monthly production which ranks it as the lowest performing system. In addition, those devices maintained stable cooling [Olimat et al. 2022, Ismail 2024; Ismail et al. 2025], along with consistent structure and performance [Ali 2024, Khalifeh, et al. 2021, Alzaareer, et al. 2025]. The findings demonstrate that maximizing energy collection procedures for April, June and October with reduced wind speeds would generate considerable power efficiency improvements.

CONCLUSIONS

The research examined and optimized low-speed wind energy harvester operations between piezoelectric wind energy harvesters and triboelectric nanogenerators to maximize power output within urban areas with wind speeds under 2 m/s. The wind speed measurements at Amman Arab University revealed an average 1.11 m/s speed level which makes conventional wind turbines ineffective thus requiring alternative energy harvesters as solutions for this context.

The wake galloping TENG generated the most power from this set of technologies because

it produced 90 mW at 1 m/s wind speed thus establishing itself as the leading solution for slow wind conditions. A benchmark double-bluff body exciter PWEH produced 25.6 mW yet variable channel TENGs and concave-convex PWEHs showed better power density although they failed to exceed wake galloping TENG power output. The Y-shaped attachments PWEH produced reduced efficiency levels because of its structural design constraints.

The optimized design strategy proved to enhance the performance output of the energy harvesting processes. Efficiency reached 80% when piezoelectric materials were selected properly as part of structural improvements that included impedance matching protocols. The optimization process for piezoelectric materials boosted the overall energy output by 20% up to 80% and the addition of impedance tuning produced a 60% increase thus validating the necessity of refining electrical parameters. The combination of structural modifications in stiffness alongside aerodynamic enhancements improved mechanical-to-electrical energy conversion while reducing wind-induced vibrations.

The variations in seasonal wind speeds significantly changed the amounts of power produced. Reaching wind speeds of 1.4 m/s during March and May resulted in optimal power generation for wake galloping TENG (1040 Wh) and Y-shaped PWEH (1035 Wh). The power generation dropped by 335 Wh when the wind speed decreased to 0.95 m/s in April and October thus demonstrating the necessity for hybrid power systems to maintain continuous electricity production.

Acknowledgement

The research was financially supported by Amman Arab University.

REFERENCES

1. Akbari A.M., Yaghoubirad M., Zareie Z., Azizi N., Goodini M.J., Tahmouresi R., et al. 2022. Piezomagnetic cantilever stator energy harvester using Savonius wind rotor. *Sustainable Energy Technologies and Assessments*, 50, 101826. <https://doi.org/10.1016/j.seta.2021.101826>
2. Ali M., Khan S.A., Ali A., Ali S., ul Hassan R., Cho D.H., et al. 2023. Low profile wind savonius turbine triboelectric nanogenerator for powering small

- electronics. *Sensors and Actuators A: Physical*, 363, 114535. <https://doi.org/10.1016/j.sna.2023.114535>
3. Ali M. 2024. Applications of nanotechnology and nanoproduction techniques. *Open Engineering*, 14(1): p. 20240063.
 4. Alzaareer K., Agha A., Salem Q., El-Bayeh C.Z., Zellagui M., and Al-Omary M., Development of voltage stability-based bus dependency matrix for modern power networks. *Energy*, 2025: p. 134875.
 5. Chung S.H., Son J., Cha K., Choi M., Jung H., Kim M-K., et al. 2023. Boosting power output of fluttering triboelectric nanogenerator based on charge excitation through multi-utilization of wind. *Nano Energy*, 111, 108389. <https://doi.org/10.1016/j.nanoen.2023.108389>
 6. Fan X., He J., Mu J., Qian J., Zhang N., Yang C., et al. 2020. Triboelectric-electromagnetic hybrid nanogenerator driven by wind for self-powered wireless transmission in Internet of Things and self-powered wind speed sensor. *Nano Energy*, 68, 104319. <https://doi.org/10.1016/j.nanoen.2019.104319>
 7. Fang Y., Tang T., Li Y., Hou C., Wen F., Yang Z., et al. 2021. A high-performance triboelectric-electromagnetic hybrid wind energy harvester based on rotational tapered rollers aiming at outdoor IoT applications. *iScience*, 24(4), 102300. <https://doi.org/10.1016/j.isci.2021.102300>
 8. Fu X., Jiang Z., Cao J., Dong Z., Liu G., Zhu M., Zhang C. 2024. A near-zero quiescent power breeze wake-up anemometer based on a rolling-bearing triboelectric nanogenerator. *Microsystems & Nanoengineering*, 10, 51. <https://doi.org/10.1038/s41378-024-00676-7>
 9. Han Q., Ding Z., Sun W., Xu X., Chu F. 2020. Hybrid triboelectric-electromagnetic generator for self-powered wind speed and direction detection. *Sustainable Energy Technologies and Assessments*, 39, 100717. <https://doi.org/10.1016/j.seta.2020.100717>
 10. Hu S., Zhao D., Sun W., Liu Y., Ma C. 2023. Investigation on galloping piezoelectric energy harvester considering the surface roughness in low velocity water flow. *Energy*, 262, Part B, 125478. <https://doi.org/10.1016/j.energy.2022.125478>
 11. Hu Y., Yang B., Chen X., Wang X., Liu J. 2018. Modeling and experimental study of a piezoelectric energy harvester from vortex shedding-induced vibration. *Energy Conversion and Management*, 162, 145-158. <https://doi.org/10.1016/j.enconman.2018.02.026>
 12. Ismail M., Ali A.M., Pereira S.C.C. 2025. Vortex generators in heat sinks: Design, optimisation, applications and future trends. *Results in Engineering*, 25, 104216. <https://doi.org/10.1016/j.rineng.2025.104216>
 13. Ismail M. 2024. Experimental and numerical analysis of heat sink using various patterns of cylindrical pin-fins. *International Journal of Thermofluids*, 23, 100737. <https://doi.org/10.1016/j.ijft.2024.100737>
 14. Jiang J., Zhang Y., Shen Q., Zhu Q., Ge X., Liu Y., et al. 2021. A self-powered hydrogen leakage sensor based on impedance adjustable windmill-like triboelectric nanogenerator. *Nano Energy*, 2021, 89, Part B, 106453. <https://doi.org/10.1016/j.nanoen.2021.106453>.
 15. Kan J., Liao W., Wang J., Wang S., Yan M., Jiang Y., Zhang Z. 2021a. Enhanced piezoelectric wind-induced vibration energy harvester via the interplay between cylindrical shell and diamond-shaped baffle. *Nano Energy*, 89, Part B, 106466. <https://doi.org/10.1016/j.nanoen.2021.106466>
 16. Kan J., Liao W., Wang S., Chen S., Huang X., Zhang Z. 2021b. A piezoelectric wind energy harvester excited indirectly by a coupler via magnetic-field coupling. *Energy Conversion and Management*, 240, 114250. <https://doi.org/10.1016/j.enconman.2021.114250>
 17. Kan J., Wang J., Meng F., He C., Li S., Wang S., Zhang Z. 2023. A downwind-vibrating piezoelectric energy harvester under the disturbance of a downstream baffle. *Energy*, 262, Part A, 125429. <https://doi.org/10.1016/j.energy.2022.125429>
 18. Kan J., Wang J., Wu Y., Chen S., Wang S., Jiang Y., Zhang Z. 2022. Energy harvesting from wind by an axially retractable bracket-shaped piezoelectric vibrator excited by magnetic force. *Energy*, 240, 122495. <https://doi.org/10.1016/j.energy.2021.122495>
 19. Khalifeh A., Darabkh K.A., Khasawneh A.M., Alqaisieh I., Salameh M., AlAbdala A., Alrubaye S., Al-assaf A., Al-HajAli S., and Al-Wardat R., Wireless sensor networks for smart cities: Network design, implementation and performance evaluation. *Electronics*, 2021. 10(2): p. 218.
 20. Kim H., Lee J., Seok J. 2022. Novel piezoelectric wind energy harvester based on coupled galloping phenomena with characterization and quantification of its dynamic behavior. *Energy Conversion and Management*, 266, 115849. <https://doi.org/10.1016/j.enconman.2022.115849>
 21. Ko H-J., Kwon D-S., Bae K., Kim J. 2022. Self-suspended shell-based triboelectric nanogenerator for omnidirectional wind-energy harvesting. *Nano Energy*, 96, 107062. <https://doi.org/10.1016/j.nanoen.2022.107062>
 22. Liao W., Wen Y., Kan J., Huang X., Wang S., Li Z., Zhang Z. 2022. A joint-nested structure piezoelectric energy harvester for high-performance wind-induced vibration energy harvesting. *International Journal of Mechanical Sciences*, 227, 107443. <https://doi.org/10.1016/j.ijmecsci.2022.107443>
 23. Lin H., He M., Jing Q., Yang W., Wang S., Liu Y., et al. 2019. Angle-shaped triboelectric nanogenerator

- for harvesting environmental wind energy. *Nano Energy*, 56, 269-276. <https://doi.org/10.1016/j.nanoen.2018.11.037>
24. Liu D., Luo J., Huang L., Chen M., Ji M., Wang Z.L., Kang J. 2025. Triboelectric nanogenerators as a practical approach for wind energy harvesting: mechanisms, designs, and applications. *Nano Energy*, 136, 110767. <https://doi.org/10.1016/j.nanoen.2025.110767>
25. Liu H., Li Y., Duan Z., Chen C. 2020. A review on multi-objective optimization framework in wind energy forecasting techniques and applications. *Energy Conversion and Management*, 224, 113324. <https://doi.org/10.1016/j.enconman.2020.113324>
26. Lu P., Ye L., Pei M., Zhao Y., Dai B., Li Z. 2022. Short-term wind power forecasting based on meteorological feature extraction and optimization strategy. *Renewable Energy*, 184, 642-661. <https://doi.org/10.1016/j.renene.2021.11.072>
27. Olimat A.N., Ismail M., Shaban N.A., Al-Salaymeh A. 2022. The effectiveness of the heat transfer fluid pipe orientation angle inside a latent heat thermal energy storage system. *Case Studies in Thermal Engineering*, 36, 102174. <https://doi.org/10.1016/j.csite.2022.102174>
28. Rahman M.T., Rana S.M.S., Maharjan P., Salaud-din M., Bhatta T., Cho H., et al. 2021. Ultra-robust and broadband rotary hybridized nanogenerator for self-sustained smart-farming applications. *Nano Energy*, 85, 105974. <https://doi.org/10.1016/j.nanoen.2021.105974>
29. Shi B., Wang Q., Su H., Li J., Xie B., Wang P., et al. 2023. Progress in recent research on the design and use of triboelectric nanogenerators for harvesting wind energy. *Nano Energy*, 116, 108789. <https://doi.org/10.1016/j.nanoen.2023.108789>
30. Wang J., Gu S., Zhang C., Hu G., Chen G., Yang K., et al. 2020. Hybrid wind energy scavenging by coupling vortex-induced vibrations and galloping. *Energy Conversion and Management*, 213, 112835. <https://doi.org/10.1016/j.enconman.2020.112835>
31. Wang J., Kan J., Gu Y., He C., Ren Z., Meng F., et al. 2023. Design, performance evaluation and calibration of an indirectly-excited piezoelectric wind energy harvester via a double-bluffbody exciter. *Energy Conversion and Management*, 284, 116969. <https://doi.org/10.1016/j.enconman.2023.116969>
32. Wang J., Zhou S., Zhang Z., Yurchenko D. 2019. High-performance piezoelectric wind energy harvester with Y-shaped attachments. *Energy Conversion and Management*, 181, 645-652. <https://doi.org/10.1016/j.enconman.2018.12.034>
33. Wang S., Liao W., Zhang Z., Liao Y., Yan M., Kan J. 2021. Development of a novel non-contact piezoelectric wind energy harvester excited by vortex-induced vibration. *Energy Conversion and Management*, 235, 113980. <https://doi.org/10.1016/j.enconman.2021.113980>
34. Wang S., Liu Y., Zhang K., Gao S. 2023. Self-powered electrocatalytic nitrate to ammonia driven by lightweight triboelectric nanogenerators for wind energy harvesting. *Nano Energy*, 112, 108434. <https://doi.org/10.1016/j.nanoen.2023.108434>
35. Yan Z., Shi G., Zhou J., Wang L., Zuo L., Tan T. 2021. Wind piezoelectric energy harvesting enhanced by elastic-interfered wake-induced vibration. *Energy Conversion and Management*, 249, 114820. <https://doi.org/10.1016/j.enconman.2021.114820>
36. Yuan S., Zeng Q., Tan D., Luo Y., Zhang X., Guo H., et al. 2022. Scavenging breeze wind energy (1–8.1 ms⁻¹) by minimalist triboelectric nanogenerator based on the wake galloping phenomenon. *Nano Energy*, 100, 107465. <https://doi.org/10.1016/j.nanoen.2022.107465>
37. Zhang D., Zhang X., Tan P., Li S., Yin P. 2024. Exploring the influence of concave-convex surface modifications on piezoelectric wind energy harvesting: A numerical analysis. *Ocean Engineering*, 311, Part 1, 118866. <https://doi.org/10.1016/j.oceaneng.2024.118866>
38. Zhang L., Meng B., Xia Y., Deng Z., Dai H., Hagedorn P., et al. 2020. Galloping triboelectric nanogenerator for energy harvesting under low wind speed. *Nano Energy*, 70, 104477. <https://doi.org/10.1016/j.nanoen.2020.104477>
39. Zhao K., Sun W., Zhang X., Meng J., Zhong M., Qiang L., et al. 2022. High-performance and long-cycle life of triboelectric nanogenerator using PVC/MoS₂ composite membranes for wind energy scavenging application. *Nano Energy*, 91, 106649. <https://doi.org/10.1016/j.nanoen.2021.106649>
40. Zhou Y., Lu P., Zhou X., Bai J., An S., Liu S., Pu X. 2024. Triboelectric wind sensors: Fundamentals, progress, and perspectives. *Nano Energy*, 131, Part A, 110209. <https://doi.org/10.1016/j.nanoen.2024.110209>
41. Zhou Z., Qin W., Zhu P., Du W. 2021. Harvesting more energy from variable-speed wind by a multi-stable configuration with vortex-induced vibration and galloping. *Energy*, 237, 121551. <https://doi.org/10.1016/j.energy.2021.121551>
42. Zhu W., Hu C., Bowen C.R., Wang Z.L., Yang Y. 2022. Scavenging low-speed breeze wind energy using a triboelectric nanogenerator installed inside a square variable diameter channel. *Nano Energy*, 100, 107453. <https://doi.org/10.1016/j.nanoen.2022.107453>
43. Zou H-X., Zhao L-C., Wang Q., Gao Q-H., Yan G., Wei K-X., Zhang W-M. 2022. A self-regulation strategy for triboelectric nanogenerator and self-powered wind-speed sensor. *Nano Energy*, 95, 106990. <https://doi.org/10.1016/j.nanoen.2022.106990>